Thermodynamics of protein destabilization in live cells

Jens Danielsson[a,1,2], Xin Mu[a,1], Lisa Lang[a], Huabing Wang[a], Andres Binolfi[b], François-Xavier Theillet[b], Beata Bekei[b], Derek T. Logan[c], Philipp Selenko[b], Håkan Wennerström[d], and Mikael Oliveberg[a,2]

[a]Department of Biochemistry and Biophysics, Arrhenius Laboratories of Natural Sciences, Stockholm University, 10691 Stockholm, Sweden; [b]In-Cell Nuclear Magnetic Resonance (NMR) Laboratory, Department of NMR-Supported Structural Biology, Leibniz Institute of Molecular Pharmacology (FMP Berlin), 13125 Berlin, Germany; [c]Division of Biochemistry and Structural Biology, Department of Chemistry, Lund University, 22100 Lund, Sweden; and [d]Division of Physical Chemistry, Department of Chemistry, Lund University, 22100 Lund, Sweden

Although protein folding and stability have been well explored under simplified conditions in vitro, it is yet unclear how these basic self-organization events are modulated by the crowded interior of live cells. To find out, we use here in-cell NMR to follow at atomic resolution the thermal unfolding of a β-barrel protein inside mammalian and bacterial cells. Challenging the view from in vitro crowding effects, we find that the cells destabilize the protein at 37 °C but with a conspicuous twist: While the melting temperature goes down the cold unfolding moves into the physiological regime, coupled to an augmented heat-capacity change. The effect seems induced by transient, sequence-specific, interactions with the cellular components, acting preferentially on the unfolded ensemble. This points to a model where the in vivo influence on protein behavior is case specific, determined by the individual protein's interplay with the functionally optimized "interaction landscape" of the cellular interior.

thermodynamics | protein stability | crowding | in vivo | NMR

Unlike their static impression in X-ray structures and textbook illustrations, some proteins are tuned to work at marginal structural stability. The advantage of such tuning is that it enables the protein to easily switch from one conformation to another, providing sensitive functional control. A well-known example is the tumor suppressor P53 whose function in gene regulation relies on a complex interplay of local folding–unfolding transitions (1). Likewise, the maturation pathway of the radical scavenger Cu/Zn superoxide dismutase (SOD1) involves a marginally stable apo species that seems required for interorganelle trafficking (2) and effective chaperone-assisted metal loading (3). As an inevitable consequence of such near-equilibrium action, however, the proteins become critically sensitive to perturbations (1): Mutation of SOD1 triggers with full penetrance late-onset neurodegenerative disease even though the causative mutations shift the structural equilibrium only by less than a factor of 3 (4). In the latter case, it is not the loss of native function that poses the acute problem, but rather the promotion of competing disordered SOD1 conformations that eventually exhaust the cellular proteostasis system and end up in pathologic deposits (5–8). Uncovering the rules, capacity and limitations of this delicate interplay between individual proteins and the cellular components (9, 10) requires not only information about the in vivo response to molecular perturbations, but also precise quantification of the structural equilibria at play. The question is then, to what extent are existing data obtained under simplified conditions in vitro transferable to the complex environment in live cells (11)? The answer is not clear cut. Defying predictions from steric crowding effects (11–13), experimental data have shown that cells in some cases stabilize (14–19) and in other cases destabilize (20–25) the native protein structures. In this study, we shed light on these seemingly conflicting results by mapping out the thermodynamic behavior of a marginally stable β-barrel protein (SOD1[barrel]), using in-cell NMR. Our results show that mammalian and bacterial cells not only destabilize SOD1[barrel], but also render its structure essentially disordered at 37 °C. The effect is assigned to transient interactions

with the cellular interior, which counterbalance the crowding pressure, narrow the width of the thermal unfolding transitions, and move both cold and heat unfolding into the physiological regime. Moreover, these transient interactions are seen to be sequence and context dependent, reconciling the previous observations that different proteins yield different results. The emerging picture is thus that proteins are optimized not only for structure and function but also for their interplay with the host-cell environment, raising interesting questions about the physiological manifestation of marginal stability, as well as the constraints on protein behavior across evolutionary diverse organisms.

Results

In-Cell Effects on the Folded State. Our model protein is the 110-residue β-barrel scaffold [Protein Data Bank (PDB) code 4BCZ] of the ubiquitous radical scavenger *Cu/Zn superoxide dismutase* (PDB code 1HL5). This SOD1 variant (SOD1[barrel]) was constructed by truncating the metal-binding loop IV and the electrostatic loop VII of the mother protein (26), which obliterates the native dimerization and leaves a catalytically inactive, well-behaved monomer that presents several advantages for in-cell analysis (Fig. S1). The SOD1[barrel] displays a simplistic two-state folding transition (26); lacks complexity in form of native metal-binding ligands (27) and cysteine moieties (28); and is extensively characterized with respect to mutational response (27, 29, 30), structural dynamics (26, 31), and aggregation behavior (6). Also, SOD1[barrel] displays fully resolved NMR spectra in mammalian cells (32). For the mammalian-cell experiments, we used the

Significance

A key question in structural biology is how protein properties mapped out under simplified conditions in vitro transfer to the complex environment in live cells. The answer, it appears, varies. Defying predictions from steric crowding effects, experimental data have shown that cells in some cases stabilize and in other cases destabilize the native protein structures. In this study, we reconcile these seemingly conflicting results by showing that the in-cell effect on protein thermodynamics is sequence specific: The outcome depends both on the individual target protein and on its detailed host-cell environment.

human ovary adenocarcinoma cell line A2780 (33), which was found to have good properties for protein delivery and sustainability in the NMR tubes. ^{15}N-labeled protein was delivered into the cytosol of mammalian cells by electroporation (*SI Materials and Methods*) and after recovery and washing, the treated cells were gently packed in an NMR tube (*SI Materials and Methods*). Intracellular SOD1^{barrel} concentrations were 20–30 μM, matching those in transgenic ALS mice (34, 35), and substantially higher than the 1- to 5-μM endogenous concentration of SOD1 in mammalian cells (36). Controls of efficiency and yield of internalization are described in *SI Controls* and Fig. S2A. The results show high-resolution in-cell heteronuclear multiple quantum coherence (HMQC) spectra of folded and freely tumbling SOD1^{barrel} molecules, matching closely those obtained in vitro (*SI Controls* and Fig. S2B). A notable effect of the internalization, however, is an increased degree of protonation of the protein's histidine side chains. By using SOD1^{I35A} itself as a pH probe, we determine the intracellular pH to 6.5 (*SI Controls* and Fig. S2C). This cytosolic acidification is expected and arises from the hypoxic conditions in tightly packed NMR tubes: The cultured cancer cells redirect their metabolism to glycolytic pathways with little effect on viability (32). The NMR cross peaks show that the acidification commences early in the experiment, is uniform across the protein population, and remains stable for more than 5 h.

Thermodynamic Analysis. Although the in-cell spectrum of folded SOD1^{barrel} can be used for establishing the cytosolic pH and basic molecular mobility, it cannot be used on its own for measurement of the folding equilibrium. Such an analysis requires simultaneous detection of both the folded (N) and denatured (D) states in free equilibrium, i.e., an unfolding titration curve (37), where the folding equilibrium (K_{D-N}) and stability (ΔG_{D-N}) are given by

$$\Delta G_{D\text{-}N} = -RT \ln K_{D\text{-}N} = \frac{-RT \ln[N]}{[D]}. \qquad [1]$$

To establish such balanced equilibrium, we destabilized SOD1^{barrel} by the core mutation I35A (SOD1^{I35A}). The mutation leaves the structure and surface unchanged (*SI Controls*, Fig. S3 *A–F*, and Table S1) but renders the protein partly unfolded under physiological conditions. As proof of principle, the NMR spectrum of SOD1^{I35A} shows mixed populations of D and N in PBS buffer at pH 6.5 and 37 °C (Fig. 1). For quantification of K_{D-N} = [N]/[D] we use the volumes of the C-terminal Q153 cross peaks, which are well separated and insensitive to temperature/viscosity-induced relaxation effects (*SI Controls* and Fig. S3 *G–L*). Upon lowering the temperature, the SOD1^{I35A} equilibrium shifts progressively toward N, displaying a thermal unfolding midpoint of T_m = 35 °C in the in vitro control (Fig. 1). At 17 °C, N reaches a maximum occupancy of 85% to finally decrease again as the temperature becomes lower still. This curved temperature dependence of K_{D-N} is a generic effect of the heat-capacity increase upon unfolding (ΔC_p) according to refs. 37 and 38,

$$\Delta G_{D\text{-}N}(T) = \Delta H_{D\text{-}N}(T_0) - T\Delta S_{D\text{-}N}(T_0)$$
$$+ \Delta C_p\left[T - T_0 - T\ln\left(\frac{T}{T_0}\right)\right], \qquad [2]$$

where ΔH_{D-N} and ΔS_{D-N} are the enthalpy and entropy of unfolding, respectively. The ΔC_p change is due to an increase in the hydrophobic hydration and provides a useful measure of the increase in solvent-accessible surface area of the N to D transition (39). Because the hydration grows "stronger" at lower temperatures, the larger surface area of D promotes cold unfolding and curved $\Delta G_{D-N}(T)$ profiles (38). For SOD1^{I35A}, the cold-unfolding midpoint is determined to T_C = −3 °C, in good agreement with independent controls based on CD data (*SI Controls* and Fig. S4 *A and B*). This
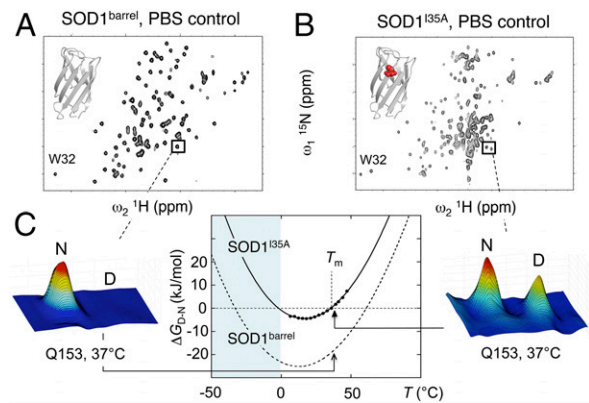

Fig. 1. In vitro benchmarking of SOD1^{barrel}, poised at marginal thermodynamic stability by the mutation SOD1^{I35A}. (*A*) HMQC spectra of SOD1^{barrel} at 37 °C, showing uniformly folded protein. *Inset* shows the X-ray structure of SOD1^{barrel} (PDB code 4BCZ), constituting the β-barrel scaffold of the parent ALS-associated protein Cu/Zn superoxide dismutase 1 (32). (*B*) Corresponding HMQC spectra of the mutant SOD1^{I35A} (PDB code 4XCR), showing mixed population of folded (N) and unfolded (D) material. Quantification of the D/N equilibrium is from the cross-peak volumes of the C-terminal resonance Q153. (*C*) ΔG_{D-N} vs. temperature profiles of SOD1^{barrel} and SOD1^{I35A} obtained from NMR thermal scans. The populations of D and N vs. temperature show melting a point T_m = 35.4 °C, i.e., ΔG_{D-N} = 0 (Eq. 1), and cold unfolding at subzero temperature. The curved ΔG_{D-N} profiles with stability maxima around room temperature are characteristic for naturally evolved proteins (58) and define a standard set of thermodynamic parameters with well-established structural meaning (Eq. 2).

thermodynamic description of SOD1^{I35A} in vitro sets the reference for quantification of the in cell effects (Table 1 and Table S2).

Cells Promote Global Unfolding of SOD1^{I35A}. Upon transfer into the mammalian A2780 cells the protein SOD1^{I35A} is clearly destabilized: At 37 °C, the folding equilibrium shifts fourfold toward the denatured state (Fig. 2 and Table 1). Notably, this effect is opposite to that expected from steric crowding (11–13) and points to the presence of attractive interactions between SOD1^{I35A} and the intracellular medium. The nature of these interactions is indicated by the temperature dependence of the in-cell stability. Inside cells, the D ⇄ N transition shows a 37% increase of ΔC_p (Table S2), resulting in a narrowing of the thermal unfolding transitions (Fig. 2). Also, the D and N species remain in dynamic equilibrium during the 4-h experiments, without significant drift of populations or loss of protein material (*SI Controls* and Fig. S4C). Because the NMR chemical shifts and line broadening suggest that the structure of internalized N remains unchanged and free of specific interactions (Fig. S3), it is reasonable to conclude that the ΔC_p increase is mainly due to in-cell modulation of D. For controls of data skewing by temperature-induced pH shifts and ionic strength, see *SI Controls* and Fig. S4 *D–H*. As an additional test, we performed in-cell experiments on SOD1^{I35A} overexpressed in *Escherichia coli* (Fig. 2). The results show that *E. coli* decreases T_m to a smaller extent than A2780 cells, but lifts the $\Delta G_{D-N}(T)$ profile to overall lower stability (Fig. 2). Coupled to this lift is a substantial increase in the cold-unfolding midpoint, which moves into the physiological regime at T_C = 8.4 ± 1.7 °C (Table 1), and the temperature for maximum SOD1^{I35A} stability shifts from 14 °C in mammalian cells to 20 °C in *E. coli* (Fig. 2, Table 1, *SI Data*, and Fig. S5 *A, H, and I*). Thus, judging by T_m alone, the mammalian cells would deceptively appear to have a smaller destabilizing effect than *E. coli*, emphasizing the importance of characterizing the whole $\Delta G_{D-N}(T)$ profile in this type of experiment. Because of higher line broadening in *E. coli* cells (Fig. S5 *H and I*), we are currently unable to accurately determine K_{D-N} = [N]/[D] below 10 °C and, hence, the precise effect on ΔC_p. From the ΔC_p increase in mammalian cells, however, it is indicated that the SOD1^{I35A} destabilization is here accompanied by increased surface area of the

Table 1. Thermodynamic parameters of the in-cell data and in vitro controls

Protein/conditions	ΔG_{D-N}*, kJ/mol	T_m, °C	T_C†, °C
SOD1^{barrel}/PBS‡	−18.6 ± 0.3	61.0 ± 0.3	−33.1 ± 1.8
SOD1^{I35A}/PBS	0.64 ± 0.12	35.6 ± 0.3	−2.1 ± 1.4
SOD1^{I35A}/in A2780 cells	4.49 ± 0.50	28.0 ± 0.5	1.1 ± 0.6
SOD1^{I35A}/in E. coli cells	2.25 ± 0.30	31.0 ± 0.7	8.4 ± 1.7
SOD1^{I35A}/ficoll 70§	−0.62 ± 0.14	38.5 ± 0.4	−7.8 ± 1.7
SOD1^{I35A}/PEG^{400}§	−0.39 ± 0.15	37.6 ± 0.2	−8.3 ± 7.2
SOD1^{I35A}/holoSOD1^{dimer}§	0.53 ± 0.14	35.6 ± 0.4	−4.0 ± 1.8
SOD1^{I35A}/BSA§	0.94 ± 0.14	34.6 ± 0.4	−6.1 ± 1.8
SOD1^{I35A}/TTHA^{pwt}§	1.02 ± 0.13	34.0 ± 0.4	−14.8 ± 3.3
SOD1^{I35A}/lysozyme¶	5.72 ± 0.29	21.2 ± 1.0	13.5 ± 2.6

For a complete set of thermodynamic parameters, see Table S2.
*At 37 °C (SI Materials and Methods).
†Negative values extrapolated from thermodynamic parameters (SI Materials and Methods).
‡Derived from CD data (SI Controls).
§Calculated at 100 mg/mL crowder concentration (SI Controls).
¶Parameters extrapolated to 100 mg/mL (SI Controls).

denatured state. The canonical structures of D, which are observed to be relatively collapsed in pure water (40), seem to expand upon interaction with the intracellular components. Such expansion is also consistent with previous observations of increased unfolding m values in E. coli (21) and increased temperature sensitivity of the protein refolding kinetics in mammalian cells (18).

Formal Description of in-Cell Interactions. Provided that the interactions between SOD1^{I35A} and the intracellular environment are overall weak, as is suggested by the NMR data, it is possible to formally describe their effect on the D ⇌ N equilibrium as follows. Assume that one has a number of cellular components {j} of concentration C_j. For each component the interaction potential with SOD1^{I35A} is given by $U_{ij}(\mathbf{r}_{ij}, \{\tau\})$, where i denotes either N or D, $\mathbf{r}_{ij}$ is the relative position of i and j, and τ denotes all other coordinates needed to describe the potential. The effect on the D ⇌ N equilibrium of the unspecific interactions $U(\mathbf{r}_{ij})$ can then be quantified using a virial expansion of the osmotic pressure and the second virial coefficient is

$$B_{ij} = -\frac{1}{N(\tau)}\int \exp\left\{\frac{-U_{ij}(\vec{r},\tau)}{kT} - 1\right\} d\tau d\vec{r}, \quad [3]$$

where $N(\tau)$ is a normalization integral over the variables $\{\tau\}$. The integral over the center of mass separation $d\mathbf{r}_{ij}$ implies that B_{ij} has the dimension of a volume. It follows from the Gibbs–Duhem relation that the chemical potential of SOD1^{I35A} in conformation i is

$$\mu_i = \mu_i^0 + kT \ln C_i + kT \sum_j B_{ij} C_j. \quad [4]$$

When we neglect higher-order terms in the virial expansion, it follows from Eq. **4** that the in-cell equilibrium constant is

$$K_{D\text{-}N}^{cell} = K_{D\text{-}N}^{ref} \exp\left\{\sum_j (B_{Nj} - B_{Dj}) C_j\right\}, \quad [5]$$

where K_{D-N}^{ref} is the in vitro reference. Thus, depending on the difference between the virial coefficients in the cell environment, either N or D can be favored. It is furthermore likely that the sum over cell components j contains both negative and positive terms, where the value of the virial coefficient B_{ij} is determined

by the intermolecular potential U_{ij} (Eq. **3**). The main repulsive contribution to the potential U_{ij} is due to the excluded volume interaction. Excluded volume is always present and gives a positive contribution to the virial coefficient, which is larger for the expanded D than for the more compact N. If this was the dominant contribution to B_{ij}, $K_{D-N}^{cell} < K_{D-N}^{ref}$ in Eq. **5** and the equilibrium would be shifted toward N. This stabilization of the species of smallest volume is often referred to as the crowding effect (11–13). In addition to the repulsive excluded-volume effect, there are also attractive terms in the intermolecular potentials, giving a negative contribution to the virial coefficient. The dominant, but not the only, attractive contributions stem from local interactions between ionic groups of opposite charge and patchy hydrophobic contacts. For SOD1^{I35A}, with a small net charge and closely spaced anionic and cationic groups, the compact N species is expected to show relatively weak local electrostatic interactions with the other cell components. In the more expanded D state, on the other hand, where the charges are spread out and spatially flexible, there are larger possibilities to find such attractive interactions, tending to make $|B_{Dj}| > |B_{Nj}|$ in Eq. **5**. The analogous argument holds for weak hydrophobic interactions where, again, the denatured ensemble will be stabilized due to its higher exposure of spatially amenable hydrophobic patches to the intracellular environment. An illustration of how the expanded D conformation shifts K_{D-N}^{cell} (Eq. **5**) by providing more opportunities for interactions with cellular components is given by the coupled equilibrium (see Fig. 4).

Clues from in Vitro Crowders. To experimentally delineate the contributions to the in-cell destabilization of SOD1^{I35A}, we mapped out the impact of a series of chemically distinct cosolutes in vitro (SI Data and Fig. S5 B–G). Consistent with predictions from excluded-volume effects (12) (Eqs. **3–5**), the "hard-sphere mimic" ficoll^{70} yields a progressive increase of SOD1^{I35A} stability (Fig. 3).
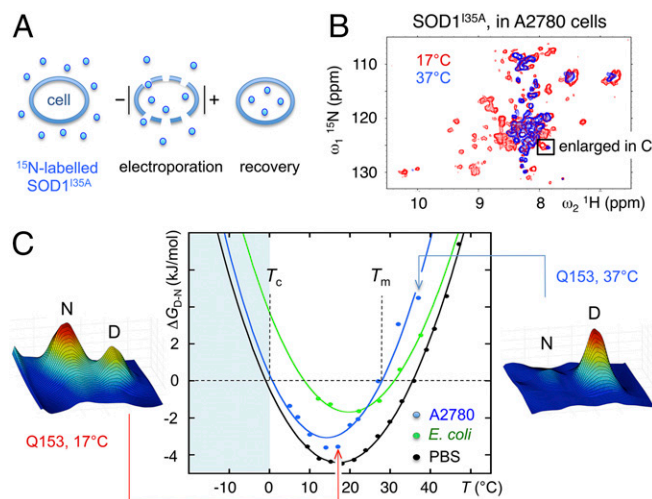

Fig. 2. In-cell quantification of protein stability. (A) Schematic illustration of protein delivery by electroporation. The method yields intracellular concentrations of SOD1^{I35A} = 20–30 µM, matching those of human SOD1 in transgenic ALS mice (43) and in vitro aggregation studies (6). (B) Two overlaid in-cell HMQC spectra of SOD1^{I35A} showing that the protein is mainly folded at 17 °C (red) and fully unfolded already at 37 °C (blue). An advantage of this detection strategy is that the target protein is retained fully physiological and devoid of potentially interfering spectroscopic reporters. (C) ΔG_{D-N} vs. temperature profiles based on quantification of the D/N equilibrium from the Q153 cross-peak volumes. The results show that both mammalian and bacterial cells substantially destabilize SOD1^{I35A}, albeit in slightly different ways. A common feature is that the in-cell destabilization shifts both cold unfolding (T_C) and melting temperatures (T_m) to the physiological regime (Table 1).

The data show, however, that the origin of this stabilization is molecularly more complex than excluded volume alone, because it is predominantly enthalpic in nature and without notable impact on ΔC_p (Table S2). This is not surprising as osmolytes in general not only occupy volume but also alter the osmotic pressure, yielding multiple components to the effect on protein stability (compare Eq. 3). Because the ficoll[70] effect contrasts with the in-cell data, the stabilizing excluded-volume/osmotic pressure contributions seem outweighed by opposing attractive interactions in live cells (Eq. 5). Next, we benchmarked PEG[400] that is reported to be an intermediate between a stabilizing osmolyte and a chemical denaturant (41). Similar to ficoll[70], PEG[400] yields an overall stabilization of SOD1[I35A] (Fig. 3), but with an accompanying increase of ΔC_p (Table S2). The latter indicates expansion of the denatured state of SOD1[I35A], consistent with the previously observed PEG[400] binding (41) and the present in-cell data (Table 1 and Table S2). To better isolate the attractive solute contributions we finally crowded SOD1[I35A] with a series of different globular proteins. The assumption is that these structurally fixed proteins represent hard spheres with variable surface properties determined by their respective amino acid composition. As a putative "strong" interacting partner we used folded lysozyme with a net positive charge (+8.5 e), allowing multiple electrostatic coordination possibilities with the negatively charged SOD1[I35A] species (−0.5 e) (Table S3). To minimize any opposing effects of excluded volume, we ran the experiments in the low-concentration regime of [lysozyme] = 0 mg/mL, 30 mg/mL, and 50 mg/mL. In contrast to the inert osmolytes, lysozyme promotes a marked destabilization of SOD1[I35A] (Fig. 3, Table 1, and Table S2). The net negative bovine serum albumin (BSA) (−8.5 e) and the bacterial putative heavy metal binding protein TTHA[pwt] (−1.5 e), on the other hand, show no or little effect on SOD1[I35A] stability, whereas the cysteine-depleted SOD1 dimer, holoSOD1[dimer] (−5 e), yields a slight stabilization (Fig. 3, Table 1, and Table S2). Taken together, these results show that the effect of surrounding proteins is variable and depends on their detailed surface features. The observation not only complies with the rule that protein–protein interactions are sequence specific, but also emphasizes that the in-cell effect depends on the sequence of the target protein itself: The attraction potential relies on all partners in play (Eq. 3).

Discussion

In-Cell Modulation of Protein Stability and Conformational Equilibria. The destabilization and unfolding of SOD1[I35A] in mammalian cells illustrate well how classical in vitro analysis can easily overlook key physiological details (Fig. 2). With the caveat that cultured A2780 cells are not neuronal tissue, the in-cell destabilization observed here would suggest that the aggregation precursor in ALS, i.e., the reduced apoSOD1 monomer with a stability similar to that of SOD1[I35A], is largely unfolded in the neurons and not partly structured as envisaged in vitro (29, 42) (SI Data and Fig. S5 J–L). Such in vivo induced unfolding also explains why soluble apoSOD1 material in spinal cord of ALS mice is fully recognized by antibodies targeting disordered peptide epitopes (43). So, what causes this stability loss? Generally, the steric crowding experienced in the cellular compartment is predicted to stabilize proteins (11, 13). However, proteins engage also in various attractive interactions as they constantly search their environment for functional partners (19, 44–46). If these interactions are on average stronger for the folded state (N), they act stabilizing, and if they are stronger for the unfolded state (D), they act destabilizing (Eqs. 3–5 and Fig. 4). A key distinction here is that, unlike steric crowding, the protein's interactions with the cellular environment depend on sequence identity (19, 45, 46), governed by the same rules as protein folding itself (47). For SOD1[I35A], our results suggest that this sequence-specific crosstalk dominates the in-cell experience.

Protein Identity and Cell Environment: Case-Specific Effects. From the perspective of sequence-specific crosstalk (attractive interactions)
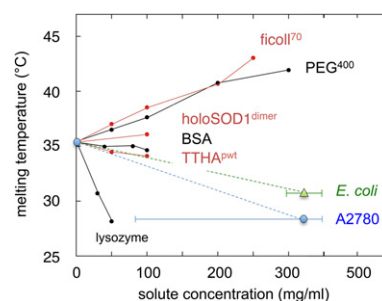

Fig. 3. Comparison of in vivo and in vitro data, showing that osmolytes yield stability changes opposite to those of the cells, whereas protein crowders yield the whole spectrum of effects, underlining the amino acid sequence dependence of the protein solute interactions. The solute concentrations of A2780 and *E. coli* cells show considerable variation in the literature (13), spanning the range of the error bars.

it is not surprising that experiments targeting different proteins in different cell types and cell lysates yield different results. For example, intracellular stabilization has been observed for the lambda repressor in *E. coli*, using MS hydrogen/deuterium (HD)-exchange analysis (14); for GB1 in *E. coli* cytosol (19) and quenched *E. coli* lysate, using NMR HD-exchange analysis (15); and for FRET-labeled Tau (16) and phosphoglycerate kinase (PGK) (17, 18) in mammalian cell lines. The effect on PGK was also seen to vary with cell type, stage of cell cycle, and intracellular localization, underlining the importance of the detailed chemical context surrounding the target protein (17, 25). At the other end of the spectrum, FLASH-labeled CRABP (20) was found to become markedly destabilized in *E. coli* (21), and ubiquitin shows increased HD exchange rates in mammalian cells, suggested to arise from transient interactions with endogenous proteins (22). Similar stability losses are revealed upon titrating of the chymotrypsin inhibitor 2 (CI2) with bacterial lysate (23), by intracellular expression of a mammalian surface antigen (24), and by the mammalian- and bacterial-cell data presented here (Fig. 3, Table 1, and Table S2). Taken together, these observations underline the universal principle of structure–function relationships: The in vivo modulation of protein stability and structural behavior is by no means uniform, but case specific, determined by the interplay between an individual protein and its cellular "encounter interactome."

Nature of the Protein–Cell Crosstalk. A ubiquitous source of in-cell interactions is the innate proteostasis system, which "buffers" structural stability and viable protein levels by a complex network of chaperones, transporters, and degradation pathways (8, 48). Somewhat surprisingly, the homogenous and temporally stable two-state equilibrium of SOD1[I35A] (SI Controls) shows that this proteostasis interference is either small or short-lived on the NMR timescale or sequesters strongly a minor, constant, fraction of the protein molecules that blinds out in the analysis and does not take part in the folding equilibrium. There is also no skewing of the $\Delta G_{D\text{-}N}(T)$ profiles (Fig. 2), indicating that the conceivable interference from the proteostasis/chaperone system changes with temperature; i.e., there is no apparent heat- or cold-shock response (48). In terms of thermodynamics, this simplistic behavior allows us to assign the SOD1[I35A] destabilization to transient interactions alone (23) (Eqs. 3–5 and Fig. 4). The interpretation is also in full agreement with the similar effect of homogenous protein solutions (Fig. 3). At present it is not possible to deduce whether our inability to distinguish specific in-cell interactions relates to the specific chaperone-binding affinities of SOD1 itself (49) or reflects a general feature of soluble two-state proteins. Nevertheless, it can be safely assumed that, at a molecular level, one of the primary modulators of weak protein interactions is the side-chain charges, which not only steer macromolecular association and encounter complexes (19, 45) but also maintain solubility by negative design (50–52). The effect
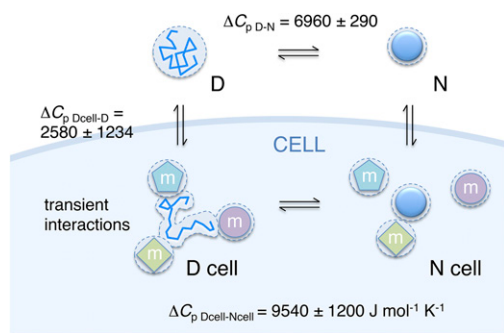
BIOPHYSICS AND COMPUTATIONAL BIOLOGY

Fig. 4. Coupled folding equilibrium describing the shift toward denatured material upon interaction with the cellular interior, as formalized in Eqs. **3–5**. Both the denatured (D) and folded (N) species interact with the cellular molecules (m), but the interactions are stronger/more numerous for the structurally expanded and flexible D species. The increased heat capacity of unfolding (ΔC_p) observed in the cellular compartment (Eqs. **1** and **2** and Fig. 2) is attributed to increased solvent-accessible surface area (dotted boundary) of the denatured ensemble (D cell), promoted by the transient association with neighboring macromolecules (m). Following Elcock's estimate (44), SOD1^{I35A} would at all times experience approximately five putative interaction partners in its immediate cellular environment. Associated thermodynamic parameters are in Table 1 and Table S2.

of lysozyme (+8.5 e) on SOD1^{I35A} (−0.5 e) could then be ascribed to net-charge attraction alone (Table 1). However, there is more to it: The stabilization induced by holoSOD1^{dimer} (−5 e) does not scale with the smaller effects of BSA (−8.5 e) and TTHA^{pwt} (−1.5 e) (Fig. 3). The phenomenon is pinpointed by Sarkar et al. who demonstrated that removal of positively charged proteins from *E. coli* lysates does not significantly reduce CI2 destabilization (53). Like macromolecular interactions in general, each in-cell encounter presents a frustrated (47) conflict between many types of protein interactions, involving also dipoles, hydrophobic contacts, and geometric compatibility. It is easy to envisage that the flexible unfolded chain is here more amenable to find productive contacts than its folded counterpart (Fig. 4).

Quantification. The realization that cells interact with their proteins in a sequence-specific manner allows rational modeling of the in vivo behavior from basic physical–chemical principles. Our results show that mammalian-cell internalization not only reduces SOD1^{I35A} stability but also increases ΔC_p and folding cooperativity: The unfolding transition becomes narrower and more responsive to temperature changes (Fig. 3, Table 1, and Table S2). Following mass action, this indicates that the in-cell environment makes the denatured state more hydrated (39). The same tendencies have previously been hinted at by increased urea *m* values in *E. coli* (21) and by increased temperature dependence of the folding kinetics in mammalian cells (18). In the simplest case, the effect stems from a conformational extension of the unfolded protein itself, perhaps as a result of the flexible chain "spanning" across dispersed interaction sites (13, 54, 55) (Fig. 4). A similar picture is captured by Elcock's full-scale simulation of the bacterial cytoplasm (44) where the stability of individual proteins either decreases or increases, depending on how the unfolded and folded material preferentially interacts with the surrounding. This intrinsic trade-off between steric crowding and weak encounter interactions explains why "passive" osmolytes like ficoll^{70} and PEG^{400} poorly mimic the physiological setting, why different proteins yield different results, and how crowding with chemically distinct proteins can induce the full spectrum of effects (Fig. 3, Table 1, and Table S2). From a theoretical perspective this is reassuring: Protein behavior in vivo seems after all defined by the mixing and environmental tweaking of individual folding funnels (47).

Physiological Occurrence of Cold Unfolding. Intriguingly, the biologically most striking effect of cell internalization is on the

cold-unfolding temperature (T_C), which increases to just above zero in mammalian cells and to +8.6 °C in *E. coli* (Table 1). This inherent, yet rarely considered, phenomenon stems from the parabolic temperature dependence of protein stability (56) and moves both the cold-unfolding and melting temperatures of SOD1^{I35A} into the physiological regime (Fig. 3 and Table 1). As analogous behavior is expected for any conformational transition involving sufficient exchange of coordinated water, it is surprising that physiological links to cold unfolding seem missing in the literature, except for an example in Antarctic fish (57). After all, some of the many proteomes of organisms adapted to low temperatures should contain members with structural properties that resemble, or partly overlap with, those of SOD1^{I35A}. Because natural two-state proteins in general are most stable around room temperature (58), the thermal behavior of SOD1^{I35A} is also expected to be representative of marginally stable proteins rather than an odd exception. Regardless of what the physiological occurrence of cold unfolding turns out to be, settling this issue will help delineate the yet poorly understood biological constraints on protein stability.

Concluding Remarks. The answer to how protein behavior in vitro translates to in vivo conditions (13, 44, 59) seems now to be gradually unfolding. Although general confinement and excluded-volume effects must contribute, the rule of the game is in the molecular details: In-cell stability depends not only on the protein sequence itself, but also on how it interacts with its specific intracellular environment. From a sequence perspective alone, different proteins are thus expected to show different in vivo behavior, as is indeed observed in a series of independent in-cell studies, using a broad range of experimental techniques (14–24). Although some of these differences likely stem from experimental and molecular variation other than protein sequence, e.g., intracellular composition, stress response, and physical–chemical variation, they bring attention to the role of organism divergence. Because protein surfaces undergo much more rapid evolution than 3D structures (60), the surfaces exposed by the proteome of bacteria and mammalian cells are not the same. This divergence is found not only in functional interfaces, but also in "background" surfaces outside specific binding epitopes (61), leading to a new balance with the molecules in the cellular medium. The question is then, How will a protein behave in a foreign cellular environment? Our observations show that indeed there is a difference: Above room temperature SOD1^{I35A} is more stable in *E. coli*, whereas at lower temperatures it is better off in the mammalian cells (Fig. 2, Table 1, and Table S2). Along the same line Gruebele and coworkers have found that, even within mammalian cell lines, protein stability depends both on the phase of the cell cycle and on organelle localization (16, 18). Even though the details of these protein–environment relationships are yet to be pinned down, it is clear that the field of physical chemistry has finally moved in vivo (14–24): Molecular phenomena that were previously limited to speculation and inference from in vitro data can now be addressed directly in the environment where proteins are evolved to function.

Materials and Methods

Protein Engineering. Mutagenesis, expression, and purification were as in refs. 26 and 28.

Protein Internalization and in-Cell Analysis. For each in-cell NMR sample, 75–100 × 10^6 cells containing 1 mM ^{15}N isotope-labeled SOD1^{I35A} were electroporated by a Super Electroporator NEPA21 (NePa Gene). Measurements were performed on a Bruker Avance 700 MHz spectrometer. ^{1}H-{^{15}N}-sofast-heteronuclear multiple quantum coherence (62) spectra were used for all in vivo and in vitro experiments. The folded and unfolded populations were determined from the volumes of the C-terminal Q153 cross peaks and ΔG_{D-N} was calculated from Eq. **1**.

Structure Determination. Crystals of SOD1^{I35A} were grown at 293 K by the sitting-drop vapor-diffusion method. Data were collected at 100 K on station I911-3 of the MAX IV Laboratory synchrotron, Lund, Sweden. Results have been deposited in the PDB, ID code 4XCR.

1. Joerger AC, Fersht AR (2008) Structural biology of the tumor suppressor p53. *Annu Rev Biochem* 77:557–582.
2. Bergemalm D, et al. (2006) Overloading of stable and exclusion of unstable human superoxide dismutase-1 variants in mitochondria of murine amyotrophic lateral sclerosis models. *J Neurosci* 26(16):4147–4154.
3. Luchinat E, et al. (2014) In-cell NMR reveals potential precursor of toxic species from SOD1 fALS mutants. *Nat Commun* 5:5502.
4. Byström R, Andersen PM, Gröbner G, Oliveberg M (2010) SOD1 mutations targeting surface hydrogen bonds promote amyotrophic lateral sclerosis without reducing apo-state stability. *J Biol Chem* 285(25):19544–19552.
5. Ciryam P, Tartaglia GG, Morimoto RI, Dobson CM, Vendruscolo M (2013) Widespread aggregation and neurodegenerative diseases are associated with supersaturated proteins. *Cell Reports* 5(3):781–790.
6. Lang L, Kurnik M, Danielsson J, Oliveberg M (2012) Fibrillation precursor of superoxide dismutase 1 revealed by gradual tuning of the protein-folding equilibrium. *Proc Natl Acad Sci USA* 109(44):17868–17873.
7. Eichner T, Kalverda AP, Thompson GS, Homans SW, Radford SE (2011) Conformational conversion during amyloid formation at atomic resolution. *Mol Cell* 41(2):161–172.
8. Balch WE, Morimoto RI, Dillin A, Kelly JW (2008) Adapting proteostasis for disease intervention. *Science* 319(5865):916–919.
9. Beckman JS, Carson M, Smith CD, Koppenol WH (1993) ALS, SOD and peroxynitrite. *Nature* 364(6438):584.
10. Hipp MS, Park SH, Hartl FU (2014) Proteostasis impairment in protein-misfolding and -aggregation diseases. *Trends Cell Biol* 24(9):506–514.
11. Zhou HX, Rivas G, Minton AP (2008) Macromolecular crowding and confinement: biochemical, biophysical, and potential physiological consequences. *Annu Rev Biophys* 37:375–397.
12. Cheung MS, Klimov D, Thirumalai D (2005) Molecular crowding enhances native state stability and refolding rates of globular proteins. *Proc Natl Acad Sci USA* 102(13):4753–4758.
13. Ellis RJ, Minton AP (2003) Cell biology: Join the crowd. *Nature* 425(6953):27–28.
14. Ghaemmaghami S, Oas TG (2001) Quantitative protein stability measurement in vivo. *Nat Struct Biol* 8(10):879–882.
15. Monteith WB, Pielak GJ (2014) Residue level quantification of protein stability in living cells. *Proc Natl Acad Sci USA* 111(31):11335–11340.
16. Dhar A, Ebbinghaus S, Shen Z, Mishra T, Gruebele M (2010) The diffusion coefficient for PGK folding in eukaryotic cells. *Biophys J* 99(9):L69–L71.
17. Dhar A, et al. (2011) Protein stability and folding kinetics in the nucleus and endoplasmic reticulum of eucaryotic cells. *Biophys J* 101(2):421–430.
18. Guo M, Xu Y, Gruebele M (2012) Temperature dependence of protein folding kinetics in living cells. *Proc Natl Acad Sci USA* 109(44):17863–17867.
19. Monteith WB, Cohen RD, Smith AE, Guzman-Cisneros E, Pielak GJ (2015) Quinary structure modulates protein stability in cells. *Proc Natl Acad Sci USA* 112(6):1739–1742.
20. Ignatova Z, et al. (2007) From the test tube to the cell: Exploring the folding and aggregation of a beta-clam protein. *Biopolymers* 88(2):157–163.
21. Ignatova Z, Gierasch LM (2007) Effects of osmolytes on protein folding and aggregation in cells. *Methods Enzymol* 428:355–372.
22. Inomata K, et al. (2009) High-resolution multi-dimensional NMR spectroscopy of proteins in human cells. *Nature* 458(7234):106–109.
23. Sarkar M, Smith AE, Pielak GJ (2013) Impact of reconstituted cytosol on protein stability. *Proc Natl Acad Sci USA* 110(48):19342–19347.
24. Guzman I, Gelman H, Tai J, Gruebele M (2014) The extracellular protein VlsE is destabilized inside cells. *J Mol Biol* 426(1):11–20.
25. Wirth AJ, Platkov M, Gruebele M (2013) Temporal variation of a protein folding energy landscape in the cell. *J Am Chem Soc* 135(51):19215–19221.
26. Danielsson J, Kurnik M, Lang L, Oliveberg M (2011) Cutting off functional loops from homodimeric enzyme superoxide dismutase 1 (SOD1) leaves monomeric β-barrels. *J Biol Chem* 286(38):33070–33083.
27. Leinartaite L, Saraboji K, Nordlund A, Logan DT, Oliveberg M (2010) Folding catalysis by transient coordination of Zn2+ to the Cu ligands of the ALS-associated enzyme Cu/Zn superoxide dismutase 1. *J Am Chem Soc* 132(38):13495–13504.
28. Lindberg MJ, Normark J, Holmgren A, Oliveberg M (2004) Folding of human superoxide dismutase: Disulfide reduction prevents dimerization and produces marginally stable monomers. *Proc Natl Acad Sci USA* 101(45):15893–15898.
29. Nordlund A, Oliveberg M (2006) Folding of Cu/Zn superoxide dismutase suggests structural hotspots for gain of neurotoxic function in ALS: Parallels to precursors in amyloid disease. *Proc Natl Acad Sci USA* 103(27):10218–10223.
30. Nordlund A, et al. (2009) Functional features cause misfolding of the ALS-provoking enzyme SOD1. *Proc Natl Acad Sci USA* 106(24):9667–9672.
31. Danielsson J, et al. (2013) Global structural motions from the strain of a single hydrogen bond. *Proc Natl Acad Sci USA* 110(10):3829–3834.
32. Danielsson J, et al. (2013) Pruning the ALS-associated protein SOD1 for in-cell NMR. *J Am Chem Soc* 135(28):10266–10269.
33. Hamilton TC, Young RC, Ozols RF (1984) Experimental model systems of ovarian cancer: Applications to the design and evaluation of new treatment approaches. *Semin Oncol* 11(3):285–298.
34. Bergh J, et al. (2015) Structural and kinetic analysis of protein-aggregate strains in vivo using binary epitope mapping. *Proc Natl Acad Sci USA* 112(14):4489–4494.
35. Lang L, et al. (2015) SOD1 aggregation in ALS mice shows simplistic test tube behavior. *Proc Natl Acad Sci USA* 112(32):9878–9883.
36. Westman NG, Marklund SL (1981) Copper- and zinc-containing superoxide dismutase and manganese-containing superoxide dismutase in human tissues and human malignant tumors. *Cancer Res* 41(7):2962–2966.
37. Tanford C (1968) Protein denaturation. *Adv Protein Chem* 23:121–282.
38. Oliveberg M, Tan YJ, Fersht AR (1995) Negative activation enthalpies in the kinetics of protein folding. *Proc Natl Acad Sci USA* 92(19):8926–8929.
39. Myers JK, Pace CN, Scholtz JM (1995) Denaturant m values and heat capacity changes: relation to changes in accessible surface areas of protein unfolding. *Protein Sci* 4(10):2138–2148.
40. Wuttke R, et al. (2014) Temperature-dependent solvation modulates the dimensions of disordered proteins. *Proc Natl Acad Sci USA* 111(14):5213–5218.
41. Senske M, et al. (2014) Protein stabilization by macromolecular crowding through enthalpy rather than entropy. *J Am Chem Soc* 136(25):9036–9041.
42. Chattopadhyay M, et al. (2008) Initiation and elongation in fibrillation of ALS-linked superoxide dismutase. *Proc Natl Acad Sci USA* 105(48):18663–18668.
43. Zetterström P, et al. (2007) Soluble misfolded subfractions of mutant superoxide dismutase-1s are enriched in spinal cords throughout life in murine ALS models. *Proc Natl Acad Sci USA* 104(35):14157–14162.
44. McGuffee SR, Elcock AH (2010) Diffusion, crowding & protein stability in a dynamic molecular model of the bacterial cytoplasm. *PLoS Comput Biol* 6(3):e1000694.
45. Schreiber G, Fersht AR (1996) Rapid, electrostatically assisted association of proteins. *Nat Struct Biol* 3(5):427–431.
46. Sugase K, Dyson HJ, Wright PE (2007) Mechanism of coupled folding and binding of an intrinsically disordered protein. *Nature* 447(7147):1021–1025.
47. Oliveberg M, Wolynes PG (2005) The experimental survey of protein-folding energy landscapes. *Q Rev Biophys* 38(3):245–288.
48. Lindquist SL, Kelly JW (2011) Chemical and biological approaches for adapting proteostasis to ameliorate protein misfolding and aggregation diseases: Progress and prognosis. *Cold Spring Harb Perspect Biol* 3(12):a004507.
49. Wang J, et al. (2009) Progressive aggregation despite chaperone associations of a mutant SOD1-YFP in transgenic mice that develop ALS. *Proc Natl Acad Sci USA* 106(5):1392–1397.
50. Otzen DE, Kristensen O, Oliveberg M (2000) Designed protein tetramer zipped together with a hydrophobic Alzheimer homology: A structural clue to amyloid assembly. *Proc Natl Acad Sci USA* 97(18):9907–9912.
51. Vendruscolo M, Dobson CM (2007) Chemical biology: More charges against aggregation. *Nature* 449(7162):555.
52. Kurnik M, Hedberg L, Danielsson J, Oliveberg M (2012) Folding without charges. *Proc Natl Acad Sci USA* 109(15):5705–5710.
53. Sarkar M, Lu J, Pielak GJ (2014) Protein crowder charge and protein stability. *Biochemistry* 53(10):1601–1606.
54. Vuzman D, Levy Y (2010) DNA search efficiency is modulated by charge composition and distribution in the intrinsically disordered tail. *Proc Natl Acad Sci USA* 107(49):21004–21009.
55. Kudlay A, Cheung MS, Thirumalai D (2012) Influence of the shape of crowding particles on the structural transitions in a polymer. *J Phys Chem B* 116(29):8513–8522.
56. Privalov PL, Makhatadze GI (1993) Contribution of hydration to protein folding thermodynamics. II. The entropy and Gibbs energy of hydration. *J Mol Biol* 232(2):660–679.
57. Todgham AE, Hoaglund EA, Hofmann GE (2007) Is cold the new hot? Elevated ubiquitin-conjugated protein levels in tissues of Antarctic fish as evidence for cold-denaturation of proteins in vivo. *J Comp Physiol B* 177(8):857–866.
58. Kumar S, Tsai CJ, Nussinov R (2002) Maximal stabilities of reversible two-state proteins. *Biochemistry* 41(17):5359–5374.
59. Frembgen-Kesner T, Elcock AH (2013) Computer simulations of the bacterial cytoplasm. *Biophys Rev* 5(2):109–119.
60. Gerstein M, Sonnhammer EL, Chothia C (1994) Volume changes in protein evolution. *J Mol Biol* 236(4):1067–1078.
61. Göbel U, Sander C, Schneider R, Valencia A (1994) Correlated mutations and residue contacts in proteins. *Proteins* 18(4):309–317.
62. Schanda P, Brutscher B (2005) Very fast two-dimensional NMR spectroscopy for real-time investigation of dynamic events in proteins on the time scale of seconds. *J Am Chem Soc* 127(22):8014–8015.
63. Becktel WJ, Schellman JA (1987) Protein stability curves. *Biopolymers* 26(11):1859–1877.
64. Collaborative Computational Project, Number 4 (1994) The CCP4 suite: Programs for protein crystallography. *Acta Crystallogr D Biol Crystallogr* 50(Pt 5):760–763.
65. Emsley P, Cowtan K (2004) Coot: Model-building tools for molecular graphics. *Acta Crystallogr D Biol Crystallogr* 60(Pt 12 Pt 1):2126–2132.
66. Dalby PA, Oliveberg M, Fersht AR (1998) Folding intermediates of wild-type and mutants of barnase. I. Use of phi-value analysis and m-values to probe the co-operative nature of the folding pre-equilibrium. *J Mol Biol* 276(3):625–646.

BIOPHYSICS AND COMPUTATIONAL BIOLOGY